

Exchange Bias Induced by the Fe_3O_4 Verwey transition

J. de la Venta^{1,*}, M. Erekhinsky¹, Siming Wang^{1,2}, K. G. West¹, R. Morales^{3,4} and Ivan K. Schuller¹

1.- *Department of Physics and Center for Advanced Nanoscience, University of California San Diego, La Jolla, CA 92093 USA*

2.- *Materials Science and Engineering Program, University of California San Diego, La Jolla, CA 92093 USA*

3.- *Dpto. de Química-Física, Universidad del País Vasco, 48940 Leioa, Spain.*

4.- *IKERBASQUE, Basque Foundation for Science, 48011 Bilbao, Spain.*

*) Corresponding author E-mail: jdelaventa@physics.ucsd.edu

Abstract

We present a study of the exchange bias in different configurations of V_2O_3 thin films with ferromagnetic layers. The exchange bias is accompanied by a large vertical shift in the magnetization. These effects are only observed when V_2O_3 is grown on top of $\text{Ni}_{80}\text{Fe}_{20}$ permalloy. The magnitude of the vertical shift is as large as 60% of the total magnetization which has never been reported in any system. X-Ray diffraction studies show that the growth conditions promote the formation of a ferrimagnetic Fe_3O_4 interlayer. The change in the easy magnetization axis of Fe_3O_4 across the Verwey transition at 120 K is correlated with the appearance of exchange bias and vertical shift in magnetization. Both phenomena disappear above 120 K, indicating for the first time a direct relationship between the magnetic signature of the Verwey transition and exchange bias.

PACS numbers: 75.70.-I, 75.30.Et, 75.60.-d

I. INTRODUCTION

Exchange bias (EB)^{1,2}, the horizontal shift of the hysteresis loop in ferromagnetic/antiferromagnetic (or ferrimagnetic) systems, is one of the most studied effects in thin film magnetism and is the basis for several applications^{3,4}. Most studies of EB in thin films were done by growing ferromagnetic (FM) layers on top of antiferromagnetic (AFM) oxides. These oxides exhibit unique properties including collective phenomena such as magnetism, ferroelectricity, superconductivity, metal-insulator transitions, enhanced photoconductivity and electron transfer^{5,6,7,8,9,10}. These materials hold great potential for revolutionary developments which may arise from the manipulation and control of novel emergent properties which are not present in ordinary semiconductors or metals. Interesting possibilities arise when FM thin films are layered with transition metal oxides that undergo a structural transition where there is a change in resistivity and magnetic properties. This transition provides an external tuning capability of the properties by changing the temperature. It affords a unique opportunity to study EB not only when the materials are cooled through the Neel temperature but also when their structure and resistivity change across the transition.

A particularly interesting class of oxides is the vanadium oxides VO_x ^{11,12,13} system. Among these phases, vanadium sesquioxide, V_2O_3 , undergoes a first-order metal-insulator transition at $T=160$ K from a low temperature antiferromagnetic insulating phase to a high temperature paramagnetic metallic phase^{14,15,16}. The crystal structure changes from monoclinic in the insulating phase to rhombohedral symmetry in the metallic phase. Electronic and structural properties of V_2O_3 thin films epitaxially grown on different sapphire ($\alpha\text{-Al}_2\text{O}_3$) planes have been extensively studied^{17,18}. Although the phase diagram¹⁶ suggests that a reduction in the metal-insulator transition may occur for some strain values, Allimi et al.¹⁸ showed how the transition temperatures of V_2O_3 films grown on $(11\bar{2}0)$ a- and (0001) c-plane sapphire were enhanced in both films.

The aim of this work is to study EB in V_2O_3 with different ferromagnetic thin films. For this purpose, different combinations of ferromagnetic (FM) and antiferromagnetic (V_2O_3) layers have been grown on $(1\bar{1}02)$ r-plane sapphire. EB has previously been observed in bilayers of V_2O_3 grown on $(11\bar{2}0)$ a- plane sapphire substrates with Co on top¹⁹. However the EB is absent when the top layer is Fe, which was attributed to the presence of a magnetically “dead” Fe layer at the interface. Additional investigations of Co, Ni and Fe on top of V_2O_3 grown on (0001) c-plane and $(11\bar{2}0)$ a- plane substrates²⁰ found EB for all of the combinations except for Fe on V_2O_3 $(11\bar{2}0)$.

Here we report the observation of substantial EB in permalloy (Py)/ V_2O_3 bilayers with a large vertical shift in magnetization never observed before in any system. From a series of well-defined experiments: i) X-ray diffraction, ii) Magnetization and magnetotransport iii) Cl_2 plasma etch, iv) annealing, v) trilayer and vi) (Ni)/ V_2O_3 and (Py)/ V_2O_3 bilayers we show that the formation of a Fe_3O_4 interfacial layer produces both effects. The results imply that the change in the easy magnetization axis occurring at the Fe_3O_4 Verwey transition is responsible for the EB and the vertical shift in the FM magnetization.

II. EXPERIMENTAL

The samples were prepared in a high vacuum sputtering deposition system with a base pressure of 1×10^{-7} Torr using ultrahigh purity (UHP) argon sputtering gas. The pressure during the deposition was 4×10^{-3} Torr. Bilayers and trilayers were deposited by RF sputtering of $\text{Ni}_{80}\text{Fe}_{20}$, Ni, and V_2O_3 targets on r-plane sapphire ($1\bar{1}02$) substrates. The different configurations are shown in figure 1. The RF magnetron power was kept at 100 W. In the case of FM/ V_2O_3 bilayer (figures 1a and 1b), the ferromagnetic layer was deposited at room temperature. Next, the temperature was increased to 750°C at $7^\circ\text{C}/\text{min}$ and the V_2O_3 layer was deposited. Finally the sample was cooled to room temperature at $7^\circ\text{C}/\text{min}$. In the case of $\text{V}_2\text{O}_3/\text{FM}$ bilayer (figure 1c), the V_2O_3 layer was deposited at 750°C . After cooling the sample to RT, the FM layer was deposited. Samples with different thicknesses for FM layers (20 nm to 60 nm) and V_2O_3 (25 nm to 100 nm) were fabricated. For the FM/ $\text{V}_2\text{O}_3/\text{FM}$ trilayers (figure 1d) the two bottom layers were deposited as explained for FM/ V_2O_3 bilayers and the top FM was deposited using two different conditions: at room temperature and at 750°C .

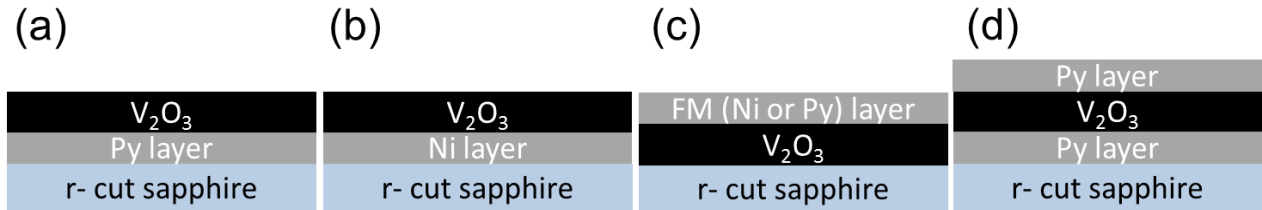


FIG. 1 (color online). Schematic model of different samples studied. (a) and (b) The Py or Ni was deposited at room temperature. The V_2O_3 layer was deposited later at 750°C after a $7\text{ K}/\text{min}$ heating ramp. (c) The V_2O_3 layer was deposited at 750°C and the top FM at room temperature (d) Trilayer used for MOKE measurements.

X-ray diffraction was performed with a Bruker D8 Discovery rotating anode X-ray diffractometer using $\text{Cu K}\alpha$ radiation.

Magnetic characterization was performed using a superconducting quantum interference device magnetometer (SQUID) and the magneto-optical Kerr effect (MOKE). While MOKE is only sensitive to the surface magnetization (the penetration length of the light is less than 50 nm for the FM layer) the SQUID measures the full magnetic moment of the sample. The samples were cooled from 250 K to 10 K in different cooling fields. Hysteresis loops were measured at various temperatures after each field cooling.

In addition, the magnetoresistance of $\text{Py}/\text{V}_2\text{O}_3$ bilayers were measured on $40\ \mu\text{m}$ wide bars etched out of the whole film using standard photolithographic techniques. Since the resistivity of V_2O_3 , even in the metallic phase, is much higher than the resistivity of FM layer, the majority of the current in the film flowed through the ferromagnetic metal layers. Therefore the anisotropic magnetoresistance (AMR) reflects the switching fields of the ferromagnetic layer.

III. RESULTS AND DISCUSSION.

A. X-ray Diffraction.

The X-ray diffraction of FM/ V_2O_3 bilayers (figure 1a and 1b) shows the following diffraction peaks (figure 2): Py or Ni in the (111) direction; V_2O_3 in the (001) direction. The Py/ V_2O_3 bilayers (figure 1a) exhibit a series of unexpected (*with instrumentally-limited widths*) diffraction peaks, marked as dots in figure 2. Two possible candidates match the X-ray diffraction peaks for this unexpected phase: V_3O_4 (111) or magnetite Fe_3O_4 (111), both with the same cubic $Fd-3m$ structure. The peak positions for (111) family planes of bulk Fe_3O_4 (or V_3O_4) are marked as lines at the top of figure 2. These unexpected diffraction maxima did not appear when the V_2O_3 thin film is deposited on top of a Ni layer. A literature review indicates that the existence of the V_3O_4 phase is uncertain. This was claimed only twice in the literature; ultra-thin, less than 1 monolayer²¹ or V_3O_4 spinel phase generated from V_2O_5 by compressive shock waves stabilized by an Fe admixture.²²

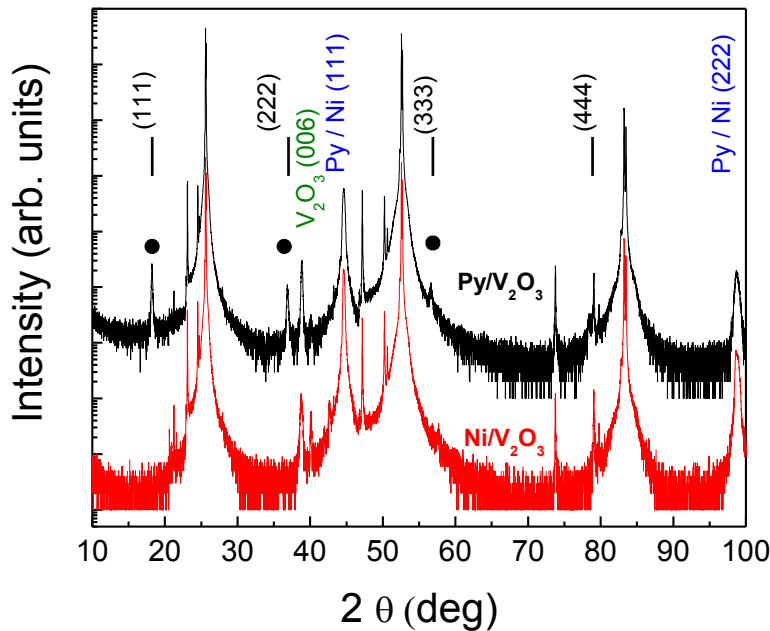


FIG. 2 (color online). X-ray diffraction patterns for two bilayers (top black) Py(30 nm)/ V_2O_3 (100 nm) ; (bottom red) Ni (30 nm)/ V_2O_3 (100 nm). Diffraction maxima from Py or Ni (111) and from V_2O_3 (006) are marked in the figure; (●) diffraction maxima from an unexpected phase. Peak positions from Fe_3O_4 or V_3O_4 (111) planes are marked at the top. All other diffraction maxima not marked in the figure are due to the r-cut sapphire substrate. Note that the (444) peak overlaps with one of the substrate peaks. See supplementary material for the substrate X-ray diffraction pattern.

B. Magnetization and Magnetotransport

Surprisingly only the Py/V₂O₃ bilayers (figure 1a) showed EB field with a large vertical shift in the magnetization (M_{Shift}), figure 3. Both the EB and M_{Shift} vanish above 120 K. No EB was found in Ni/V₂O₃ bilayers (figure 1b). In addition, bilayers with the reverse configuration, i. e. V₂O₃ at the bottom and FM (Py or Ni) on top (figure 1c) show no EB. Hence, the presence of EB is related with an interaction between the bottom Py layer and the top V₂O₃ thin film.

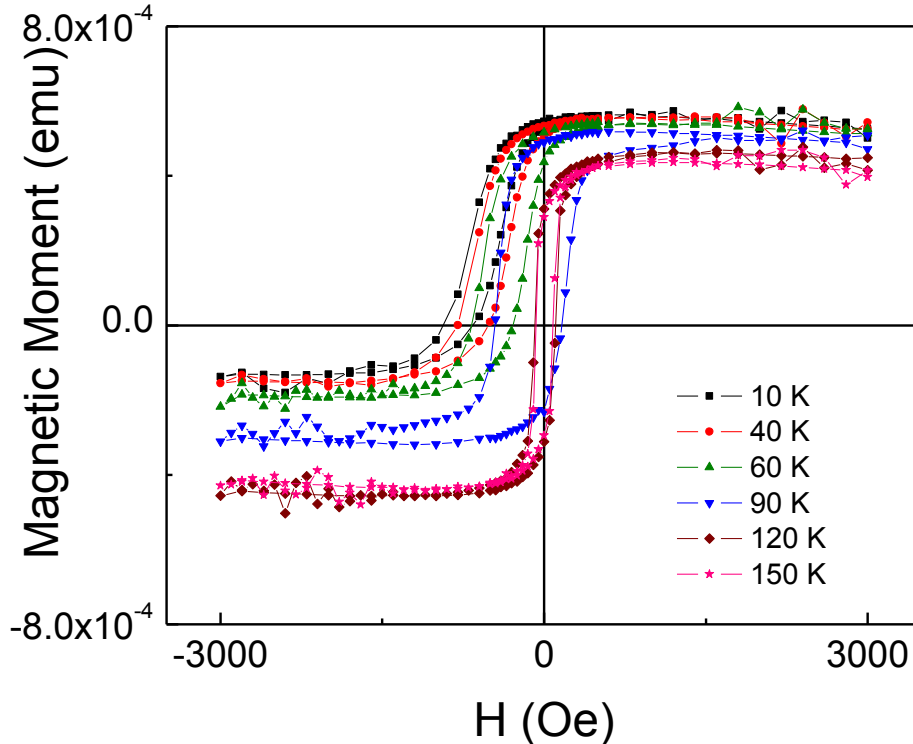


FIG. 3 (color online). Hysteresis loops at different temperatures in Py (30 nm)/V₂O₃ (100 nm) bilayers. The sample was cooled from room temperature to 10 K with a field of 1000 Oe.

The most striking effect is the large vertical shift, up to 60% of the total magnetization at 10 K, for Py (30 nm)/V₂O₃ (100 nm), black triangles in figure 4. Such large magnetization shifts were never reported in any system. In FeF₂-Fe bilayers, the shift of the hysteresis loop is about 1% of the total magnetization.²³ X-ray magnetic circular dichroism shows, a small vertical offset in Co/Ir₂₀Mn₈₀ bilayers, indicating that only a 7 % of the total uncompensated moments were pinned.²⁴ The large vertical shift in the Py/V₂O₃ bilayers indicates the presence of a large number of pinned spins. The influence of the field cooling has been investigated at fields of up to 5 T. In all cases, the shift of the hysteresis loop is “upwards” for positive cooling fields. No dependence of the M_{Shift} with the magnitude of the cooling field or indication of positive EB was found. These findings imply that the coupling between the different layers is ferromagnetic.²³ Samples with 25 nm of V₂O₃ show no EB or M_{Shift} , red squares in figure 4.

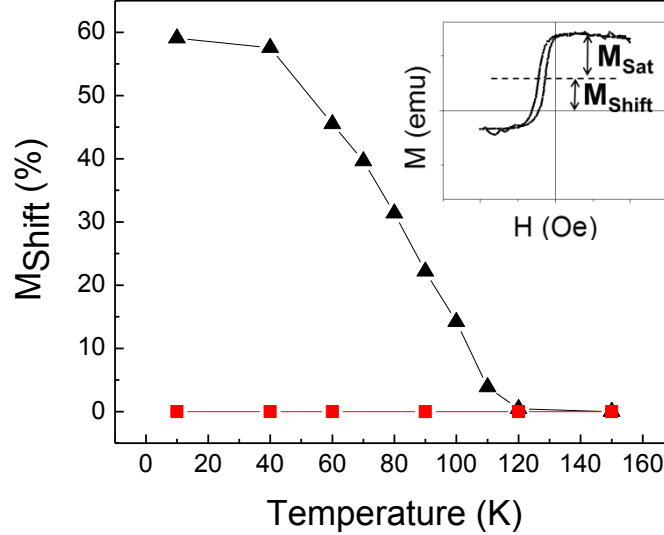


FIG. 4 (color online). Vertical shift in the magnetization (M_{Shift}) values as a function of the temperature for bilayers of different thicknesses, Py (30 nm) / V_2O_3 (y): \blacktriangle (100 nm); \blacksquare (25 nm). M_{Shift} is absent for the 25 nm V_2O_3 film. The cooling field value was 1000 Oe. (Inset) M_{Shift} (%) has been calculated from the shift of the loop with respect to the abscissa axis and normalized to the values of the saturation M_{Sat} at positive fields.

Magnetoresistance (MR) measurement of Py (30 nm)/ V_2O_3 (50 nm) bilayers confirmed the presence of EB in samples containing Py/ V_2O_3 interfaces. After the sample was cooled to 4.2 K in 1000 Oe positive magnetic field the magnetoresistance was measured at different monotonically increasing temperatures. Figure 5 shows the H field dependence of resistance at different temperatures. For each temperature there are two curves corresponding to different magnetic field sweep directions.

Below 100K the MRs are centered around a non-zero field, indicating the presence of EB. As the magnetic field is swept from a positive to negative (or vice versa) then the distance between minima in the MR indicates the coercivity of the FM layer. At 5 K and 20 K the curves match giving the same values of EB. At 100K, the bilayer MR is almost symmetric around zero field and the midpoint of the MR gradually shifts towards negative field. This indicates that the blocking temperature obtained from the MR is around 100 K.

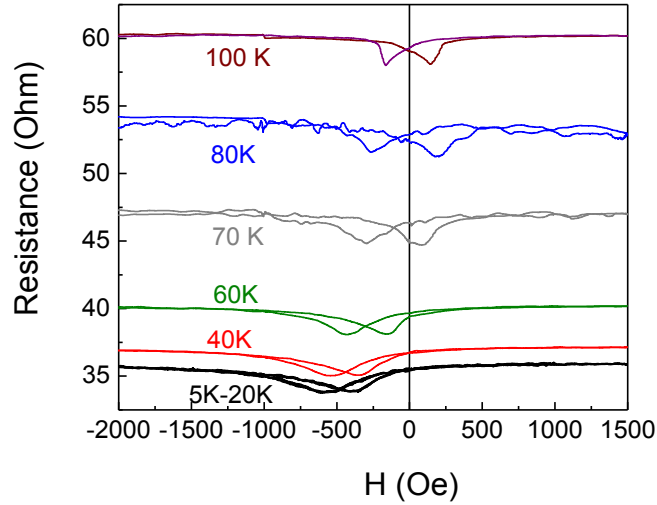


FIG. 5 (color online). Magnetoresistance measurements at different temperatures in Py (30 nm)/V₂O₃ (50 nm). The sample was cooled from 300 K to 4.2 K with an applied field of 1000 Oe.

The temperature dependence of the exchange bias (H_{EB}) and coercivity (H_C) for 30 nm of Py and different V₂O₃ thicknesses are plotted in figure 6. The H_{EB} and H_C extracted from SQUID and MR measurements are in good quantitative agreement for Py (30 nm)/V₂O₃ (50 nm), solid and empty circles in figure 6. The H_{EB} and H_C are slightly larger for the bilayer with a thicker V₂O₃ film (100 nm), indicating that it is not only due to a surface effect.²⁵ The blocking temperature, i. e. the temperature at which the EB disappears is 120 K in all cases. When the thickness of the V₂O₃ layer is 25 nm neither EB nor M_{Shift} have been observed, red squares in figures 6 and 4 respectively.

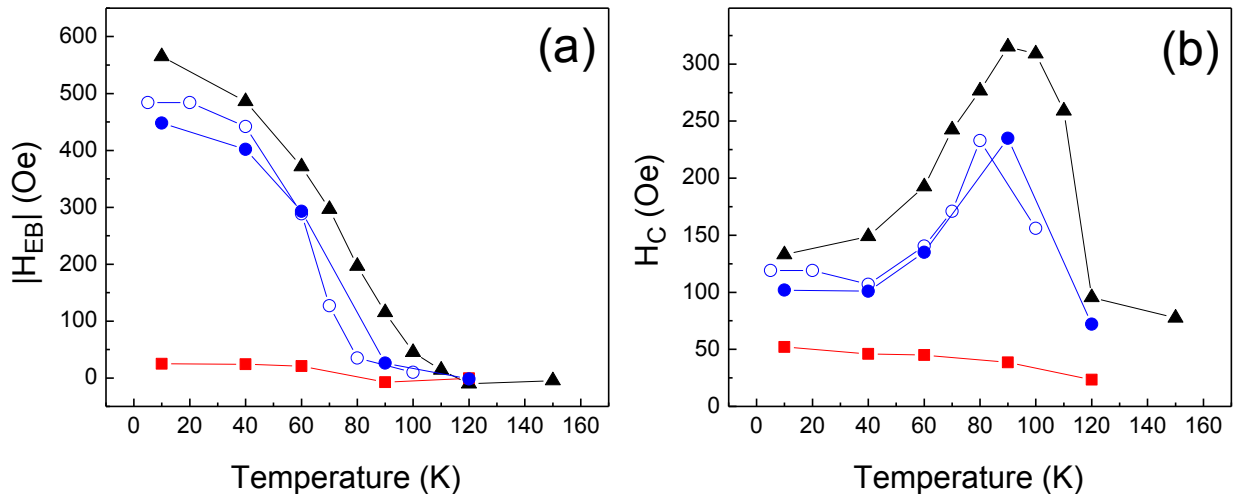


FIG. 6 (color online). (a) Dependence of the exchange bias field with temperature; (b) dependence of the coercive field with temperature. (—▲—) Py (30 nm)/V₂O₃ (100 nm) bilayers measured with SQUID; (—●—) Py (30 nm)/V₂O₃ (50 nm) measured with SQUID; (—○—) Py (30 nm)/V₂O₃ (50 nm) from magnetoresistance measurements; (—■—) Py (30 nm)/V₂O₃ (25 nm) measured with SQUID.

C. Cl_2 plasma etch.

To investigate the cause of the EB and to clarify the origin and composition of the unexpected phase found from X-ray diffraction, (figure 2) one of the samples was subjected to reactive ion etching. The Cl_2 plasma quickly etches vanadium and its oxides but not Py. The V_2O_3 (006) X-ray diffraction peaks disappear after etching, figure 7, whereas the diffraction maxima arising from the new phase remain. After etching the EB was still present with H_{EB} and M_{Shift} as in the virgin samples. This indicates that the unexpected phase is Fe_3O_4 rather than V_3O_4 .

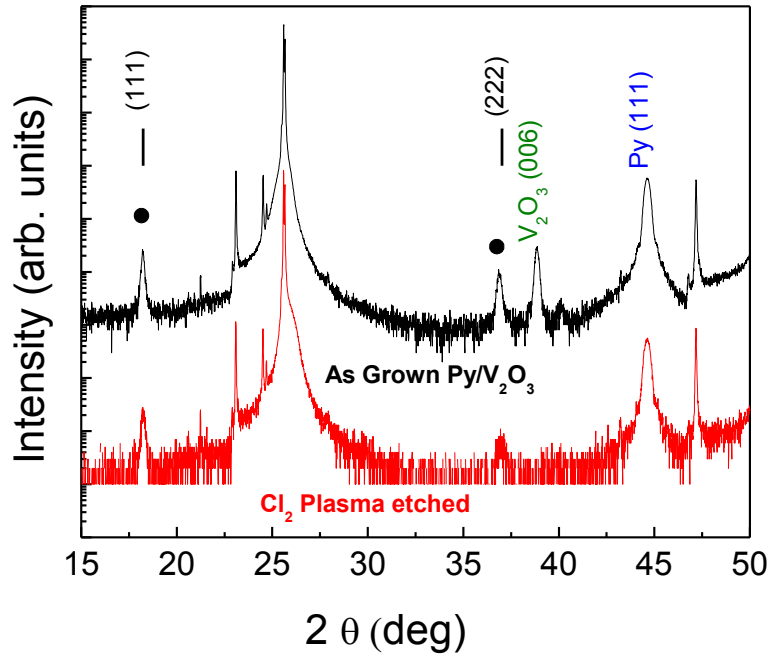


FIG. 7 (color online). X-ray diffraction patterns for a bilayer Py(30 nm)/ V_2O_3 (100 nm) (top black) as grown; (bottom red) after etching. Diffraction maxima from V_2O_3 and Py are labeled in the figure; (●) diffraction maxima from an unexpected phase. Peak positions from Fe_3O_4 (111) planes are marked at the top. All other diffraction maxima not marked in the figure are due to the r-cut sapphire substrate.

D. Annealing.

Figure 8a shows the diffraction maxima at 36.86° from Fe_3O_4 (222) and at 38.84° from V_2O_3 (006). Figure 8b shows the peaks at 44.6° from Py (111). Bilayers with 30 nm Py and different thicknesses of V_2O_3 are included. For better visualization the X-ray data have been smoothed and XRD intensity in figure 8a is plotted in linear scale whereas in figure 8b the vertical scale is logarithmic. (For raw data is See Supplemental Material).

The Py (30 nm)/ V_2O_3 (25 nm) bilayer which did not show EB or M_{Shift} (red squares in figures 4 and 6) shows V_2O_3 (006) XRD peaks but not those from the unexpected phase, figure 8a. Hereafter we refer to this sample as the unreacted bilayer. As an additional test this bilayers was subjected to thermal treatment. After depositing the

V_2O_3 layer on top of Py the temperature was kept at 750°C for 18min 45 sec (25 min total at 750°C). This is the same deposition time for 100nm V_2O_3 at which the heater was at 750°C for 25min. After this annealing, both the new diffraction maxima (figure 8a) and EB appeared. The short deposition time (4 min 15 sec) for a 25 nm V_2O_3 sample is not enough to produce the interface reaction giving rise to the Fe_3O_4 interfacial layer. However, stopping the deposition but maintaining the temperature provides the conditions for the Fe_3O_4 layer formation. The Fe_3O_4 (222) peaks in the samples with 50 nm and 100 nm V_2O_3 have the same intensity and sharpness. This is an additional indication that the thickness of the Fe_3O_4 layer is similar in both cases. As expected the peak from V_2O_3 (006) has a higher intensity in 100 nm of V_2O_3 . The intensity from the 38.84° peak for the unreacted bilayer indicates that the V_2O_3 thickness is between those bilayers with 50 and 100 nm of V_2O_3 .

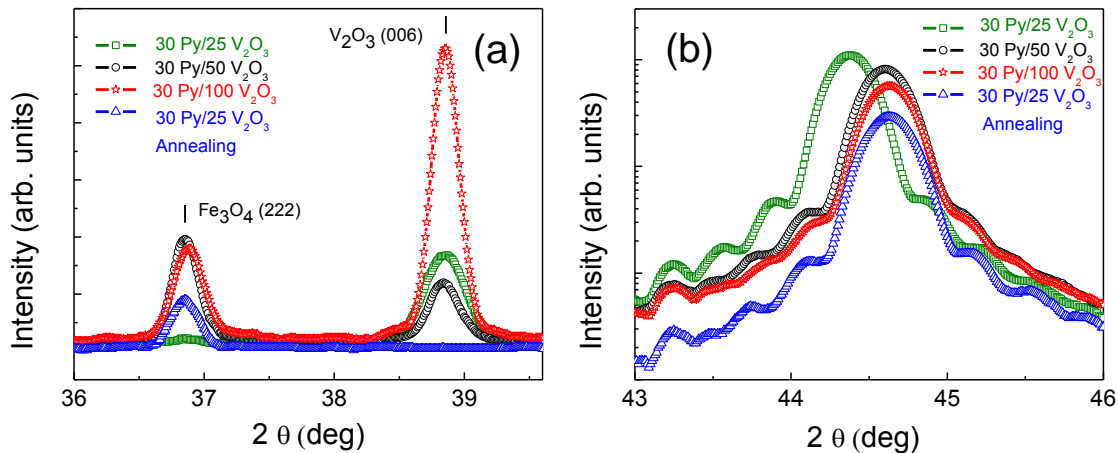


FIG. 8 (color online). X-ray diffraction patterns focused around the maxima from: (a) Fe_3O_4 (222) and V_2O_3 (006); (b) Py (111). \square —30 nm Py/25nm V_2O_3 ; \circ —30 nm Py/50 nm V_2O_3 ; \star —30 nm Py/100 nm V_2O_3 ; \triangle —30 nm Py/25 nm V_2O_3 annealed. The Fe_3O_4 (222) is located at 36.86°; the V_2O_3 (006) at 38.84°; the Py peaks shifts from 44.38° from to 44.6° and 44.63°.

The peaks close to 44.5°, figure 8b, provide further clues regarding the interface reaction of the Py film. In all the bilayers the peak position shifts (gradually) towards higher angles (44.6°, 44.63°) away from the unreacted bilayer (44.38°). The corresponding lattice parameters are 3.5124 Å, 3.5147 Å and 3.5312 Å. The latter is closer to the Py bulk value 3.5507 Å while the first are closer to the bulk Ni value 3.5238 Å. The finite size Laue oscillations around the Bragg peak for the unreacted sample are more intense and clearer than the ones of the reacted samples indicating that the interfaces are sharper. The finite size oscillations imply that the Py thickness is 28 nm for the unreacted bilayer as opposed to 23-24 nm for the rest of the samples. Thus the Py thickness is reduced approximately 5 nm by the reaction. Thus the unreacted sample shows a smoother Py surface and a lattice parameters closer to bulk Py. When reaction to form Fe_3O_4 takes place the surfaces become rougher and the lattice parameter changes closer to bulk Ni. All the above suggests Fe migration from Py to form the Fe_3O_4 layer.

E. Trilayers

MOKE measurements on Py (30 nm)/ V₂O₃ (100 nm) /Py (30 nm) trilayers (figure 1d) grown on double side polished sapphire are shown in figure 9. MOKE measurements are only sensitive to surface magnetization since the light penetration length in the FM layer is about 50 nm. Note that MOKE is not a measure of the absolute M value so it can only confirm the presence of EB field but not the vertical shift in the magnetic moment. In agreement with the previous ideas EB is only found in the bottom layer, figure 9. As a further check, EB is absent for either the top Py layer deposited at room temperature or even at 750° C. Thus, the Fe₃O₄ (111) interface is created when the V₂O₃ is deposited on top of the Py.

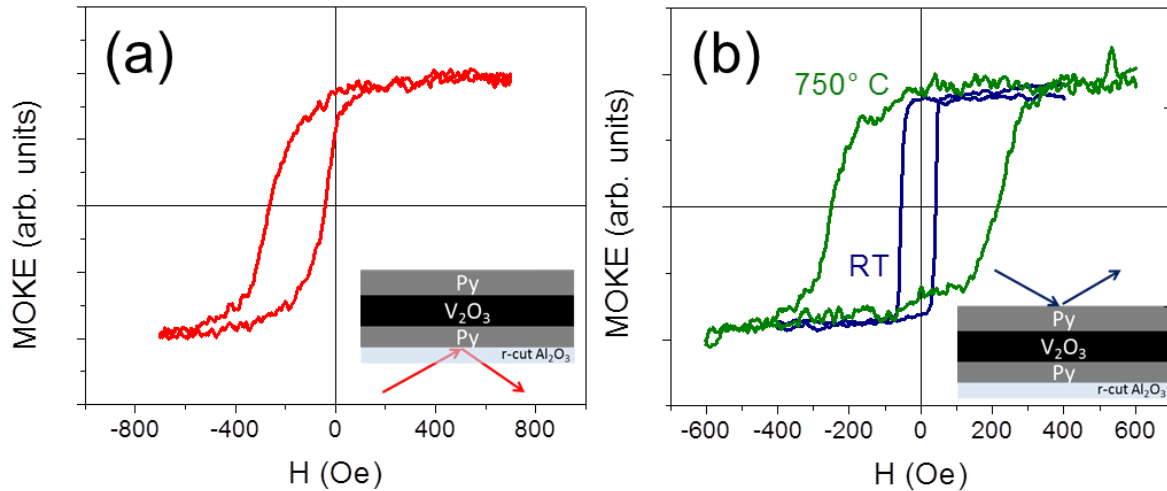


FIG. 9 (color online). MOKE hysteresis loops at 10 K after cooling the sample with a field of 1000 Oe. (a) MOKE probing bottom Py layer. (b) MOKE probing top Py layer deposited at room temperature and at 750° C. Insets: MOKE probing each FM individual layer.

Although the top Py layer exhibits no EB independently of the deposition temperature its properties are different when deposited at room temperature than 750 °C. For room temperature deposition the top layer has the characteristic metallic shiny aspect of metals. Whereas at higher temperature the surface becomes opaque thus the reflected laser intensity is somewhat reduced and the MOKE signal is noisier, figure 9b. Moreover the coercive field of this top layer is smaller for room temperature deposition, (figure 9b) which also implies smoother interfaces. The XRD data (see supplementary material) shows that the Fe₃O₄ and V₂O₃ interlayers are formed either when the top layer is deposited at room temperature or at 750° C.

F. Discussion.

All the extensive experimental evidence discussed above, shows that an unexpected interfacial phase is formed by interfacial diffusion or reaction. There are three timescales which are relevant: A) Short deposition times, without Fe₃O₄ formation; the Py preserves its bulk-like characteristics, the surfaces are smoother (figure 8b) and the

V_2O_3 deposited on top of Py “survives”. This latter point explains also the reason for the V_2O_3 peak intensities being larger for 30 nm V_2O_3 than 50 nm. B) Intermediate deposition times, causing interface reaction between the Py and V_2O_3 to form the Fe_3O_4 layer. The Py lattice parameter changes closer to bulk Ni and the interfaces become rougher. A similar process to medium deposition times occurs when annealing the samples for longer periods after deposition. In this case the 25 nm V_2O_3 layer is destroyed during the process (figure 8a) giving rise to the formation of Fe_3O_4 C) Longer deposition time, after the reaction takes place the Fe_3O_4 and Py thicknesses and their lattice parameters are stable and V_2O_3 continues growing on the newly formed Fe_3O_4 .

All the magnetic data is consistent with the EB and the M_{Shift} being caused by the magnetic interaction between the Py and an interfacial Fe_3O_4 . Further evidence is provided by the fact that when V_2O_3 is deposited on a Ni layer, neither EB nor the presence of the new Fe_3O_4 phase were found.

Fe_3O_4 is a ferrimagnetic material with a Curie temperature of 825 K which changes lattice symmetry and exhibits a metal-insulator transition at ~ 120 K (T_V), the Verwey transition.^{26, 27} The change in crystal structure is accompanied by magnetization changes. The blocking temperature for EB found here coincides with the Fe_3O_4 Verwey transition and is substantially lower than the 160K AFM transition of the V_2O_3 as shown in figure 6a. This again indicates that the EB and M_{Shift} vanishing above 120 K should be attributed to the Fe_3O_4 Verwey transition. Earlier measurements using magnetite Fe_3O_4 showed EB which vanishes at 200 K and 275 K, due to antiphase boundaries²⁸ and a spin-glass-like phase²⁹, respectively. FM/ Fe_3O_4 bilayers showed EB,^{30,31} with smaller values of H_{EB} and no M_{Shift} without indications of a blocking temperature. On the other hand, the EB found in AFM/ Fe_3O_4 bilayers is attributed to presence of the AFM phase^{32,33}. To the best of our knowledge this is the first direct observation of EB which is correlated with the appearance of the Verwey transition in Fe_3O_4 .

Although the Verwey transition is known for more than 70 years, its origin is still controversial. The consensus is that the magnetic signature of the Verwey transition manifests as a shift of the easy magnetization axis from the [111] to the [100] direction.^{34,35,36,37} On the other hand, some claim that the two transitions are uncoupled and refer to the slightly higher (130 K) magnetic transition temperature as the “isotropic point” of Fe_3O_4 .^{38,39} A recent report shows that the small Fe_3O_4 lattice distortion in the c direction may account for the change in magnetic easy-axis from cubic [111] to [001] at temperatures less than T_V .⁴⁰ This debate is beyond the scope of the present paper. Since here the Fe_3O_4 grows in the (111) orientation, above 120 K the easy magnetization [111] axis is perpendicular to the FM easy axis. Thus above 120 K there is no magnetic coupling between the two layers with the consequent absence of EB and the M_{Shift} , figure 10a. Below 120 K, the easy axis of Fe_3O_4 changes to the [100] direction at 45° with the Py as shown in the inset of figure 10b. Therefore the non zero in plane magnetization component of Fe_3O_4 coincides with the easy in plane axis of the FM layer, giving rise to the EB and the M_{Shift} , figure 10b. The bilayers studied here are textured as proven clearly by the X-ray diffraction data and the cartoons just reflect the magnetic orientation in textured samples.

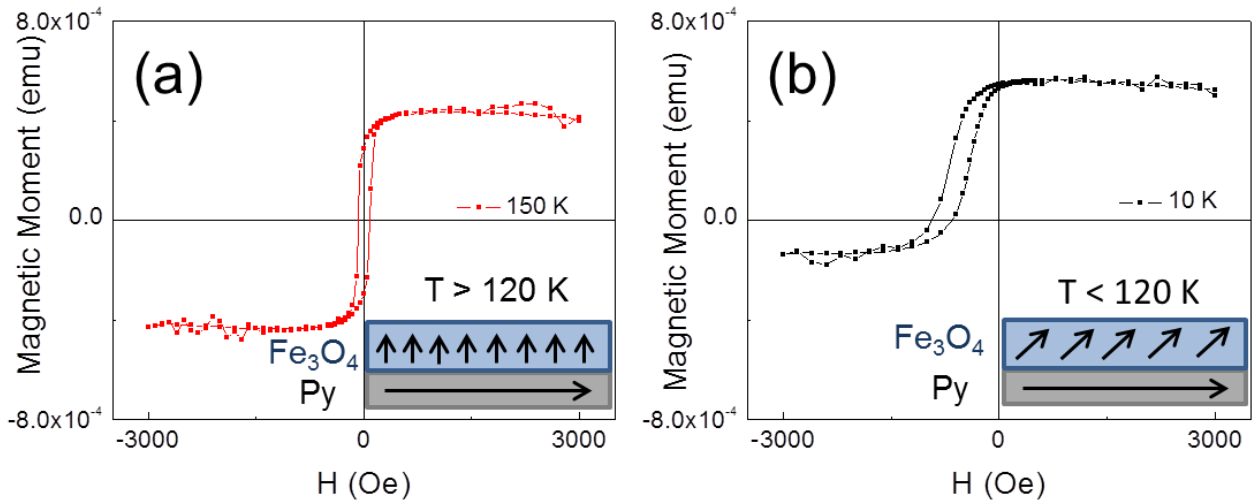


FIG. 10 (color online). Hysteresis loops in Py (30 nm)/V₂O₃ (100 nm) bilayers after field cooling at: (a) 150 K and (b) 10 K. (Insets) Simplified magnetization easy axes configuration of the Py/Fe₃O₄ bilayer: (a) [111] above the transition (b) [100] and below the transition.

IV. CONCLUSION

We studied the magnetic properties of FM/V₂O₃ bilayers grown on r-cut sapphire in a variety of configurations. The exchange bias in Py/V₂O₃ is accompanied by a large (60%) positive vertical shift in the magnetization, indicating the presence of a substantial number of pinned spins. A series of experiments show these effects are related to the formation of a Fe₃O₄ ferrimagnetic interfacial layer. The magnetic signature of the Fe₃O₄ Verwey transition at 120 K coincides with EB blocking temperature. The large EB and the M_{Shift} are produced by an interfacial ferromagnetic coupling due to changes in the Fe₃O₄ magnetic anisotropy. This is the first observation in which the magnetic signature of the Verwey transition is directly responsible for the presence of exchange bias.

ACKNOWLEDGEMENTS

This work has been supported by the US Department of Energy, Office of Basic Energy Sciences, Division of Materials Sciences under Award FG03-87ER-45332. J. de la Venta acknowledges the support of a postdoctoral fellowship from *Ministerio de Educacion* of Spain. R. M. acknowledges support from Spanish grant MICINN FIS2008-06249 and funding from IKERBASQUE Basque Foundation for Science

¹ W. H. Meiklejohn and C. P. Bean, Phys. Rev. **102**, 1413 (1956).

² J. Nogués and Ivan K. Schuller, J. Magn. Magn. Mater. **192**, 203 (1999).

³ J. C. S. Kools, IEEE Trans. Magn. **32**, 3165 (1996).

⁴ C. Tang, J. Appl. Phys. **55**, 2226(1984).

⁵ P. Perna, D. Maccariello, M. Radovic, U. Scotti di Uccio, I. Pallecchi, M. Codda, D. Marré, C. Cantoni, J. Gazquez, M. Varela, S. J. Pennycook, and F. M. Granozio, Appl. Phys. Lett. **97**, 152111 (2010).

⁶ J. Ventura, I. Fina, C. Ferrater, E. Langenberg, L. E. Coy, M. C. Polo, M. V. García-Cuenca, L. Fàbrega, and M. Varela, Thin Solid Films **518**, 4692 (2010).

⁷ M. Gich, J. Gazquez, A. Roig, A. Crespi, J. Fontcuberta, J. C. Idrobo, S. J. Pennycook, M. Varela, V. Skumryev, and M. Varela, Appl. Phys. Lett. **96**, 112508 (2010).

-
- ⁸ J. W. Seo, E. E. Fullerton, F. Nolting, A. Scholl, J. Fompeyrine, and J.-P. Locquet, *J. Phys: Condens. Matter* **20**, 264014 (2008).
- ⁹ C. Rossel, M. Sousa, C. Marchiori, J. Fompeyrine, D. Webb, D. Caimi, B. Mereu, A. Ispas, J. P. Locquet, H. Siegwart, R. Germann, A. Tapponnier, and K. Babich, *Microelectronic Engineering* **84**, 1869 (2007).
- ¹⁰ A. Scholl, J. Stöhr, J. Lüning, J. W. Seo, J. Fompeyrine, H. Siegwart, J.-P. Locquet, F. Nolting, S. Anders, E. E. Fullerton, M. R. Scheinfein, and H. A. Padmore, *Science* **287**, 1014 (2000).
- ¹¹ J. B. Goodenough, *Prog. Solid State Chem.* **5**, 145 (1971).
- ¹² W. Bruckner, H. Oppermann, W. Reichelt, J. I. Terukow, F. A. Tschudnowski, and E. Wolf, *Vanadium Oxide* (Akademie-Verlag, Berlin, 1983).
- ¹³ M. Imada, A. Fujimori, and Y. Tokura, *Rev. Mod. Phys.* **70**, 1039 (1998).
- ¹⁴ F. J. Morin, *Phys. Rev. Lett.* **3**, 34 (1959).
- ¹⁵ E. M. Page and S. A. Wass, *Vanadium: Inorganic and Coordination Chemistry*, *Encyclopedia of Inorganic Chemistry* (John Wiley & Sons, 1994).
- ¹⁶ D. B. McWhan, J. P. Remeika, T. M. Rice, W. F. Brinkman, J. P. Maita, and A. Menth, *Phys. Rev. Lett.* **27**, 941 (1971).
- ¹⁷ B. Sass, C. Tusche, W. Felsch, N. Quaas, A. Weismann, and M. Wenderoth, *J. Phys.: Condens. Matter* **16**, 77 (2004).
- ¹⁸ B. S. Allimi, S. P. Alpay, C. K. Xie, B. O. Wells, J. I. Budnick, and D. M. Pease, *Appl. Phys. Lett.* **92**, 202105 (2008).
- ¹⁹ B. Sass, C. Tusche, W. Felsch, F. Bertran, F. Fortuna, P. Ohresser, and G. Krill, *Phys. Rev B* **71**, 014415 (2005).
- ²⁰ B. Sass, S. Buschhorn, W. Felsch, D. Schmitz, and P. Imperia, *J. Magn. Magn. Mater* **303**, 167 (2006).
- ²¹ A. Maetaki, M. Yamamoto, H. Matsumoto, and K. Kishi, *Surf. Sci.* **445**, 80 (2000).
- ²² The International Centre for Diffraction Data (ICDD), *Powder Diffraction File* (PDF) number 00-034-0615.
- ²³ J. Nogués, C. Leighton, and Ivan K. Schuller, *Phys. Rev B* **61**, 1315 (2000).
- ²⁴ H. Ohldag, A. Scholl, F. Nolting, E. Arenholz, S. Maat, A. T. Young, M. Carey, and J. Stöhr, *Phys. Rev. Lett.* **91**, 017203 (2003).
- ²⁵ R. Morales, Zhi-Pan Li, J. Olamit, Kai Liu, J. M. Alameda, and Ivan K. Schuller, *Phys. Rev. Lett* **102**, 097201 (2009)
- ²⁶ E. J. W. Verwey, *Nature* **144**, 327 (1939).
- ²⁷ Friedrich Walz, *J. Phys.: Condens. Matter* **14**, R285 (2002).
- ²⁸ S. K. Arora, R. G. S. Sofin, A. Nolan, and I. V. Shvets, *J. Magn. Magn. Mater* **286**, 463 (2005)
- ²⁹ W. B. Mi, J. J. Shen, E. Y. Jiang, and H. L. Bai, *Acta Mater.* **55**, 1919 (2007).
- ³⁰ D. V. Dimitrov, A. S. Murthy, G. C. Hadjipanayis and C. P. Swann, *J. Appl. Phys.* **79**, 5106 (1996).
- ³¹ K. W. Lin, P. H. Kol, Z. Y. Guo, H. Ouyang, and J. van Lierop, *J. Nanosci. Nanotechnol.* **7**, 265 (2007).
- ³² B. Mauvernay, L. Presmanes, C. Bonningue, and Ph. Tailhades, *J. Magn. Magn. Mater.* **320**, 58 (2008).
- ³³ C. A. Kleint, M. K. Krause, R. Höhne, T. Walter, H. C. Semmelhack, M. Lorenz, and P. Esquinazi, *J. Appl. Phys.* **84**, 5097 (1998).
- ³⁴ R. Prozorov, T. Prozorov, S. K. Mallapragada, B. Narasimhan, T. J. Williams, and D. A. Bazylinski, *Phys. Rev. B* **76**, 054406 (2007).
- ³⁵ Michael G. Chaplinea and Shan X. Wang, *J. Appl. Phys.* **97**, 123901 (2005).
- ³⁶ R. Aragon, *Phys. Rev. B* **46**, 5334 (1992).
- ³⁷ E. Lima Jr., A. L. Brandl, A. D. Arelaro, and G. F. Goya, *J. Appl. Phys.* **99**, 083908 (2006).
- ³⁸ V. V. Gridin, G. R. Hearne, and J. M. Honig, *Phys. Rev. B* **53**, 15518 (1996).
- ³⁹ F. D. Stacey and S. K. Banerjee, *The Physical Principles of Rock Magnetism* (New York: Elsevier, 1974)
- ⁴⁰ M. S. Senn, J. P. Wright, and J. P. Attfield, *Nature* **481**, 173 (2012).